Published in final edited form as:
*J Mater Chem C Mater Opt Electron Devices*. 2013 April 7; 1(13): 2448–2454. doi:10.1039/C3TC00639E.

# Quantitative X-ray Absorption and Emission Spectroscopies: Electronic Structure Elucidation of $Cu_2S$ and CuS

**Prashant Kumar**[1], **Rajamani Nagarajan**[1], and **Ritimukta Sarangi**[2]

Rajamani Nagarajan: rnagarajan@chemistry.du.ac.in; Ritimukta Sarangi: ritis@slac.stanford.edu

[1]Materials Chemistry Group, Department of Chemistry, University of Delhi, Delhi, India, 110007 Fax: +91-11-27666606; Tel: +91-27662650

[2]Stanford Synchrotron Radiation Laboratory, SLAC National Accelerator Laboratory, Menlo Park, CA 94025, USA. Fax: 650-926-4100; Tel: 650-926-4621

## Abstract

The electronic structures of $Cu_2S$ and CuS have been under intense scrutiny, with the aim of understanding the relationship between their electronic structures and commercially important physical properties. Here, X-ray absorption and emission spectroscopic data have been analyzed using a quantitative, molecular orbital (MO) based approach to understand the electronic structure of these two complex systems. $Cu_2S$ is shown to have a significant amount of $Cu^{2+}$ sites and therefore $Cu^0$ centers. The presence of low-valent Cu is correlated with the electrical conductivity of $Cu_2S$, especially at high temperatures. CuS is shown to have tetrahedral $Cu^{2+}$ and trigonal $Cu^{1+}$ sites, with crystal planes that have alternating high and low charge on the Cu centers. These alternating charges may contribute to internal energy transitions required for photoluminescence properties. The in-depth electronic structure solutions presented here not only solve a complicated much-debated problem, but also demonstrate the strength of quantitative MO based approach to X-ray spectroscopies

## 1. Introduction

Copper sulfides are economically important ores that have found widespread use in various technologies, including solar cell devies, nonlinear optical material, lithium ion batteries, nanometer-scale switches, and gas sensors.[1–4] They vary widely in composition ($Cu_xS_y$) and are also present as non-stoichiometric compounds. CuS and $Cu_2S$ can be considered as end members of the stoichiometric copper sulfide family.[1,5] Despite their simple chemical formula, both $Cu_2S$ (chalcocite) and CuS (covellite) have complex structures, and several experimental and theoretical studies have attempted to understand their electronics and bonding.[6–13] CuS has a hexagonal crystalline structure, consisting of alternating layers of planar $CuS_3$ triangles, and $CuS_4$ tetrahedra. While CuS is a stable composition, $Cu_2S$ is unstable towards the formation of Cu vacancies, even in thermodynamic equilibrium with bulk Cu metal. The inherent instability of $Cu_2S$ and high mobility of its Cu centers has been exploited for controlled removal of Cu from $Cu_2S$ and for the generation of the known stoichiometries in the Cu-S system.[14] Room temperature $Cu_2S$ is monoclinic with a complex structure containing 96 copper atoms in a unit cell.[15] The crystallographic characterization



Correspondence to: Ritimukta Sarangi, ritis@slac.stanford.edu.

†**Electronic Supplementary Information (ESI) available:** EXAFS data and fits for $Cu_2S$ and CuS. Figure showing the effect of self-absorption on Cu K-edge XAS data. Details of DFT and TD-DFT calculations for simulation of the XES data. Analysis of the Cu L-edge XAS data for CuS, $[Cu(TMPA)(OH_2)](ClO_4)$ and $[(Cu[HB(3,5\text{-}Pr^i{}_2pz)_3)]_2(S_2)]$. See DOI: 10.1039/b000000x/

of intermediate $Cu_{2-x}S$ (between $Cu_2S$ and CuS) systems has been difficult due to the positions of the copper atoms within the close-packed sub lattice of S atoms, which are not well-defined.

Interestingly, important transitions in properties are observed depending on the metal to sulfur ratio in $Cu_{2-x}S$ systems. $Cu_{2-x}S$ remains diamagnetic for x = 0.0 to 0.2[12], although the reported magnetic behaviour of CuS differ markedly. CuS and $Cu_{1.8}S$ exhibit photoluminescence, which is not observed for stoichiometric $Cu_2S$.[14, 16] A large variation in electrical conductivity with composition has also been observed.[12] Only CuS exhibits morphology dependent photocatalytic properties.[17] Recent studies show that $Cu_{1.8}S$ is a good thermoelectric material.[18] The presence and variation in these important properties warrants a thorough correlation of the electronic structure with the complex crystal structures of $Cu_{2-x}S$ systems. X-ray absorption spectroscopy (XAS) has been extensively used as a tool to determine the electronic and geometric structure of materials.[19–21] However, the overwhelming number of publications on hard x-ray XAS have focused on the geometric structure, and only qualitative evaluation of the electronic structures has been performed. In this study, we investigate the Cu and S K-edge XAS and Cu XES data using a quantitative molecular orbital (MO) theory based approach to solve the long-standing debate about their electronic structures and to correlate these with their interesting physical properties.

## 2. Materials and Methods

### 2.1 Sample Preparation

Polycrystalline samples of $Cu_2S$ and CuS were prepared as previously reported.[16] The samples were flame sealed in glass ampules and sent to SSRL for measurement. The ampules were transferred into a glove box and maintained under a moisture free, ~1 ppm $O_2$ atmosphere. For the Cu K-edge XAS and XES measurements, polycrystalline samples were finely ground with BN into a homogeneous mixture and pressed into a 1 mm aluminum spacer between 37 μm Kapton windows. The samples were immediately frozen and stored under liquid $N_2$. During data collection, the samples were maintained at a constant temperature of ~10 K using an Oxford Instruments CF 1208 liquid helium cryostat. For S K-edge XAS studies, polycrystalline samples were finely ground inside a glove box using an agate mortar and pestle and a thin layer was applied on S-free 37 μm Kapton tape placed on an aluminum frame. The samples were protected from exposure to air by a 5 μm polypropylene window placed over the front of the aluminum frame over the sample. Samples were transported using sealed jars to the beamline and exposure to air was minimized during sample holder transfer into a He purged data measurement chamber.

### 2.2 Cu K-edge XAS

Cu K-edge XAS spectra for $Cu_2S$ and CuS were measured on the 20 pole, 2 T wiggler beamline 7-3 at the Stanford Synchrotron Radiation Lightsource (SSRL) under standard ring conditions of 3 GeV and ~300 mA ring current. A Si(220) double-crystal monochromator was used for energy selection. Other optical components used for the experiments were a cylindrical Rh-coated bent focusing mirror. Spectra were collected in the fully tuned configuration of the monochromator. Data were collected in transmission mode using an ionization chamber placed downstream of the sample. Internal energy calibration was accomplished by simultaneous measurement of the absorption of a Cu foil placed between two ionization chambers situated after the sample. The first inflection point of the foil spectrum was set at 8980.3 eV. Spectra presented here are 5 scan and 4 scan averages for $Cu_2S$ and CuS, respectively, which were sufficient to obtain a good signal to noise ratio in the EXAFS region. A second-order polynomial was fit to the pre-edge region and subtracted

from the entire spectrum as background. A three-region spline of orders 2, 3, and 3 was used to model the smoothly decaying post-edge region. The data were normalized using the Pyspline[22] program by subtracting a cubic spline and assigning the edge jump to 1.0 at 9000 eV. Theoretical EXAFS signals, $\chi(k)$, were calculated using *FEFF*[23, 24] (Macintosh version 8.4) and the X-ray crystal structure of $Cu_2S$ and CuS. The theoretical models were fit to the data using EXAFSPAK.[25] The structural parameters varied during the fitting process were the bond distance (R) and the bond variance $\sigma^2$, which is related to the Debye-Waller factor resulting from thermal motion, and static disorder of the absorbing and scattering atoms. The non-structural parameter $E_0$ (the energy at which the photoelectron wave vector $k$ is 0) was also allowed to vary but was restricted to a common value for every component in a given fit. Coordination numbers were systematically varied in the course of the fit but fixed within a given fit.

### 2.3 Cu K-edge XES

Cu K-edge XES data on $Cu_2S$ and CuS were measured on the 54 pole, 1 T wiggler beamline 6-2. A liquid nitrogen cooled double crystal Si(111) monochromator was used to set the incident energy at 12 keV. Vertical and horizontal focusing mirrors were used to achieve a beam size of 200 × 800 μm. Energy calibration was achieved using a Cu foil. The first inflection point of the foil spectrum was set at 8980.3 eV. Kβ X-ray emission spectra were measured using the 440 reflection of five spherically bent (R = 1 m) Si crystal analyzers in combination with a silicon drift detector aligned in a Rowland geometry, as described previously.[26] The overall energy bandwidth of the X-ray emission spectrometer was 2 eV. The data were normalized with respect to the Kα line intensity. The $K\beta_{1,3}$ and the $K\beta_{2,5}$ spectra were measured separately using different regions with significant overlap between the two regions for accurate merging of the two data sets. Significantly higher number of $K\beta_{2,5}$ scans were required to achieve similar signal quality.

### 2.4 S K-edge XAS

S K-edge XAS data were collected on the 20-pole 2T wiggler unfocussed beamline 4-3 under standard ring operating conditions of 3 GeV and ~300 mA ring current. A Si(111) double crystal monochromator was used for energy selection. Upstream optics include a Ni-coated vertically collimating and harmonic rejection mirror. A big challenge at the S K-edge with fluorescence data collection on solid samples with high sulfur compositions is self-absorption. To avoid self-absorption, the samples were ground with BN, further diluted by mixing with mineral oil and spread on the sulfur free tape as a thin layer. Room temperature measurements were performed on the sample in fluorescence mode using a Lytle detector. The sample was monitored for potential effects of beam damage and photoreduction. No beam-damage was observed over the period of data collection and the first and the last scans were superimposable for both samples. The S K-edge spectra presented herein are devoid of any oxidized sulfur contamination, which would lead to intense features in the S K-edge spectra at higher energies. For example, sulfate, which is a likely candidate in a degraded samples appears at ~2482 eV. No feature was observed in that energy range, which confirms the purity of the samples. Energy calibration was achieved using $Na_2S_2O_3.5H_2O$ as the calibrant, which was run at intervals between sample scans. The first peak of the $Na_2S_2O_3.5H_2O$ spectrum was fixed at 2472.02 eV. A second-order polynomial was fit to the pre-edge region and subtracted from the entire spectrum as background. The data were normalized using the Pyspline[22] program by subtracting a cubic spline and assigning the edge jump to 1.0 at 2490 eV. The areas under the pre-edge peaks were fit using the EDG_FIT subroutine in EXAFSPAK.[25] The pre-edge and rising-edge features were modeled with pseudo-Voigt line-shapes with a fixed 1:1 Lorentzian/Gaussian ratio.

# 3 Results and Analysis

## 3.1 Cu K-edge XAS

Cu K-edge XAS spectra for CuS and $Cu_2S$ are shown in Figure 1A. The Cu K-rising edge region (8980 to 9000 eV) includes the dipole allowed 1s→4p transition, charge transfer shakedown transitions from Cu-ligand covalent overlap, and long-range multiple scattering transitions.[20, 27, 28] Although a true understanding of all electronic factors affecting the rising-edge energy has yet to be achieved, it has been empirically observed that the energy of the rising-edge shifts to higher energy with an increase in oxidation state.[29] The rising edge for $Cu_2S$ and CuS occur at 8982.2 eV and 8984.4 eV, respectively. This 1.2 eV increase indicates an increase in the oxidation state of Cu in CuS. However, based on previous XAS, XPS and EPR studies, both $Cu_2S$ and CuS have been described as Cu(I) complexes with little or no Cu(II) character.[6, 30, 31]

To address this issue and to investigate the potential increase in oxidation state on going from $Cu_2S$ to CuS, the Cu K-edge data for discreet Cu(II) complexes are considered in Figure 1B, and energies are tabulated in Table 1. The rising-edge energy position for a bona-fide Cu(II) complex $[Cu(TMPA)(OH_2)](ClO_4)_2$ (1, ⎯) with light atom ligands (N and O) occurs at 8988.2 eV.[28] As we increase the number of coordinated sulfur atoms to the Cu center (with no change in oxidation state), the edge shifts to lower energy. For plastocyanin (2, ⎯) (1 Cu-S bond) the rising edge occurs at 8986.3 eV and for $[((TMEDA)Cu)_2(S_2)_2](OTf)_2$ (3, ⎯) (2 Cu-S bonds) the rising edge occurs at 8985.1 eV.[27, 32] In CuS, which has sites with both 4 Cu-S and 3 Cu-S bonds (see section 3.3), the edge is shifted to even lower energy and occurs at 8984.4 eV (—). This trend shows that heavy atom coordination (such as S) to the absorbing Cu center shifts the rising edge to lower energy. This shows that comparison of rising-edge data for oxidation state determination should be done on like-ligand systems only. For example, without consideration of ligand type, the over 2 eV energy difference between 1 and 3, (both Cu(II) systems), could erroneously be attributed to an oxidation state change. The Cu K-edge data for CuS and a Cu(I) complex ($[Cu(pyridine)_4](ClO_4)$ (4, ⎯))[33] (see Figure 1B) show closely spaced rising-edge energy positions. Such a comparison might have been erroneously used in the past to support a Cu(I) assignment in CuS. However, a correct comparison can only be made between $Cu_2S$ and CuS (same ligand systems), which points to increase in oxidation state and significant amount of Cu(II) in CuS.

Figure 1A (inset) shows the second derivative spectra of the expanded pre-edge region. In first row transition metal complexes with unoccupied 3d levels, a weak pre-edge transition is observed just below the onset of the intense rising-edge. This is an electric-dipole forbidden quadrupole-allowed 1s→3d transition.[34] For Cu(II) systems, a transition to the singly unoccupied ($3d^9$ configuration) orbital results in a pre-edge at ~8979 eV (typically ~100 times weaker than the rising-edge). Figure 1A shows a very weak transition at ~8979 eV for $Cu_2S$. Due to its low intensity, this transition is barely evident in the second derivative spectra and is likely attributed to a small amount (<5%) oxidized Cu species. In CuS, the pre-edge feature is significantly more intense and is shifted to higher energy (8979.5 eV). The presence of a pre-edge feature in CuS indicates $3d^9$ ($Cu^{2+}$) character.

## 3.2 S K-edge XAS

It has been amply demonstrated in discreet transition metal-S systems, that orbital overlap between a 3d valence hole with an appropriate S 3p orbital results in a pre-edge feature in the S K-edge spectrum.[36] This feature is due to a transition from the S 1s to S 3p orbital, which has gained hole character from covalent delocalization into the metal, and therefore, its occurrence directly indicates the presence of 3d hole character in the metal. As an

example, the Cl K-edge XAS spectrum of $[CuCl_4]^{2-}$ has an intense pre-edge feature (reflecting the empty $3d_{x^2-y^2}$ orbital in $Cu^{2+}$), whereas $[ZnCl_4]^{2-}$ has none (reflecting the filled $3d^{10}$ character of $Zn^{2+}$).[37] This technique has been applied to S K-edge XAS, where the energy position of the pre-edge feature has been used to determine the oxidation state of the transition metal.[36] Here, this approach is applied to $Cu_2S$ and CuS.

The S K-edge XAS spectra of $Cu_2S$ (red) and CuS (black) are presented in Figure 2(i). The inset shows the second derivative spectra. In $Cu_2S$, there are three dominant features at 2470.1, 2473.2, and 2475.0 eV (Table 1). The spectrum of CuS is richer with 5 dominant features at 2469.9, 2470.7, 2472.0, 2474.4, 2476.8 eV. In order to understand the spectral differences and rigorously assign these transitions to electronic states, it is important to first evaluate the geometric structure of both complexes. $Cu_2S$ is monoclinic and can be approximated as hexagonal close packed sulfur atoms with mobile and trigonally bonded Cu centers (scheme 1). A close inspection of the crystal structure shows that there is no interaction between the sulfur atoms (shortest S-S ~3.72 Å). Thus, the sulfur atoms in $Cu_2S$ are true monosulfide species. Equipped with this structural information, we used spectra for $Na_2S$ (monosulfide, —) as the S K-edge standard. This alkali metal monosulfide has no covalent interaction with the S centers and no pre-edge features in the S K-edge XAS data.

Figure 2(ii) shows a comparison of the experimental $Cu_2S$ data, relevant peaks (obtained from pseudo-Voigt fits to the data) and spectra of the corresponding free ligand $Na_2S$. It has been previously shown that metal binding leads to a decrease in intensity and shift to higher energy of S transitions.[35] This shift in energy is due to increase in positive charge on the S due to delocalization of negative charge into the metal center. A similar shift of the S features is observed on going from $Na_2S$ to $Cu_2S$ (see Table 2). In addition, a reasonably intense low-lying pre-edge feature is observed at 2470.1 eV. As discussed above, the low-energy feature at 2470.1 eV, could *only* be present if a metal based 3d hole delocalizes with the S 3p orbitals, unambiguously demonstrating the presence of $Cu^{2+}$ ($3d^9$) ions.

The crystal structure of CuS is more complicated, with alternating planes of trigonal and tetrahedral Cu centers. Two-thirds of the Cu centers are in tetrahedral geometry whereas one-third of the centers are in trigonal planar geometry and bound to monosulfide species only. Thus a second standard, $Na_2S_2$ (—, representing the disulfide) was included in the analysis. Figure 2iii show a comparison of the CuS S K-edge XAS data and relevant peaks (obtained from pseudo-Voigt fits) with $Na_2S$ and $Na_2S_2$, respectively. These data clearly show signatures of *both* disulfide (peak C) and monosulfide (peak D and F) in the spectrum of CuS. As expected, both these signatures shift to higher energy and become diminished in intensity relative to the standards. In addition, two distinct pre-edge features are observed at lower energy (A and B), which arise due to covalent interaction of a $Cu^{2+}$ center with the two different types of sulfur species: disulfide $(S_2)^{2-}$ and monosulfide $(S)^{2-}$. Because the $S_2^{2-}$ (−1 formal charge on S) has a lower lying 1s orbital relative to $S^{2-}$ (−2 formal charge on S), the higher energy pre-edge feature corresponds to the $S_2^{2-}$ 3p orbital delocalized with the $Cu^{2+}$ hole (see scheme 1).

### 3.3 Cu Kβ XES

X-ray absorption spectroscopy probes empty molecular levels.[38] To obtain a complete one-electron picture of the ground state, we measured the Cu X-ray emission spectra of $Cu_2S$ and CuS to examine the filled levels of Cu (directly) and S (indirectly). The data are presented in Figure 3. The $K\beta_{1,3}$ spectra (Figure 3A) for $Cu_2S$ and CuS are very similar, with the intense transition at 8907.5 eV resulting from Cu 3p to 1s emission. This emission leads to a multi-electron spin flip in the Cu 3d level, giving rise to the formally forbidden low energy shoulder at 8905.3 eV.[39] At lower energy is a transition at ~8900 eV for both $Cu_2S$ and CuS. In Fe and Mn containing systems, this feature has been related to 3p-3d

exchange interaction.[26, 40] It has been shown that in S=0 species, this features merges into other weak final states, to the lower energy side. The obvious presence of this feature demonstrates that unpaired spin density is present in both CuS and $Cu_2S$, attributable directly to the presence of $Cu^{2+}$ sites.

The $K\beta_{2,5}$ spectra (Figure 3B), which are composed of multiple features, show two dominant peaks at 8977. 6 eV and 8980.7 eV. A quantitative analysis of the $K\beta_{2,5}$ spectra has only been developed for molecular systems using density functional theory and will not be attempted here because the systems have crystalline repeating units, and as shown by XAS studies, has a mixture of different oxidation states. However, the Kβ" region, which results from a ligand 3s to Cu 1s emission can be used to distinguish the ligand types. The Kβ" (3B inset) feature for $Cu_2S$ occurs at 8968.6 eV, and that for CuS is a broader feature with a peak maxima at 8969.2 eV. A DFT simulation using simple two- and three-atom models (Figure S3) shows that the Kβ" line for $[Cu\text{-}S_2]^-$ is ~0.9 eV higher than for $[Cu\text{-}S_2]^-$. Because both Cu-S and $Cu\text{-}S_2$ features are present in CuS, the Kβ" spectra is shifted to higher energy and is broader. This also confirms the evidence from S K-edge XAS that the sulfide ($S^{2-}$) and disulfide ($S_2^{2-}$) are present as discreet units with individual bonding to the Cu sites.

## 4 Discussion

### 4.1 Electronic Structure of $Cu_2S$

All experimental data presented above show that $Cu_2S$ has $Cu^{2+}$ centers. But an interesting quantitative difference is observed between the Cu and S K-edge data. The Cu K-edge energy position and near absence of a pre-edge feature indicate the dominant presence of low-valent species ($Cu^{1+}/Cu^0$ and small contribution from $Cu^{2+}$), whereas the large S K-edge pre-edge intensity indicates the presence of significant $Cu^{2+}$ species. This is because in the presence of a mixture of Cu oxidation states, only the $Cu^{2+}$ centers that have strong covalent interaction with S have S K pre-edge features, the low-valent Cu do not contribute to the data and hence the signature of the $Cu^{2+}$ feature is large. On the other hand, all Cu oxidation states contribute to Cu K-edge, obfuscating the signal from the already weak pre-edge feature.

Importantly, the presence of $Cu^{2+}$ centers indicates that for charge compensation, an equal number of sites must be in $Cu^0$ state (the possibility of the electron on the disulfide, making a perdisulfido $S_2^{3-}$ moiety, as the S-S bond is very short; ~2.07 Å). Note that no $Cu^0$ ($3d^{10}4s^1$) feature is expected in the S K-edge data and apart from the low Cu K-edge energy of $Cu_2S$, no direct evidence for $Cu^0$ is available (since there are no reference data for non-metallic $Cu^0$ systems). Thus, the electronic structure of $Cu_2S$ is $[(m\text{-}n/_2)Cu^{2+}][(m\text{-}n/_2)(Cu^0)](nCu^+)(mS^{2-})$, (where $m\text{-}n/_2$ is small). The complex crystal structure of $Cu_2S$ precludes further quantitation of m and n.

Although, $Cu_2S$ has a heavily delocalized lattice system and charge delocalization between $Cu^0$ and $Cu^{2+}$ is expected, it is important to note that this description is distinct from one where charge delocalization results in a $Cu^{1+}$ only system. Such a delocalized electronic structure will not lead to the S K-pre-edge feature or the low-energy feature in the Cu K-XES data.

As mentioned in Scheme 1, there are two types of trigonal Cu centers in $Cu_2S$, one between the sulfide layers and one within the hcp sulfide layers.[41] Combining this with the electronic structure description developed here, a direct explanation for an important physical property of $Cu_2S$ evolves. At elevated temperatures, $Cu_2S$ has unusually mobile Cu centers, which make it a partially ionic conductor. Based on the results shown here, it is proposed that the

mobile Cu centers are dominantly in the $Cu^0$ state (between the layers) and account for the unusual conductivity of $Cu_2S$. The $Cu^{2+}$ sites remain bound to the sulfide lattice (within the layers).

### 4.2 Electronic Structure of CuS

Quantitative Cu and S K-edge XAS and Cu Kβ XES data analysis show that CuS contains discreet $Cu^{2+}$, $Cu^+$, $S^{2-}$ and $S_2^{2-}$ species. These results are in contrast to previous EPR and XPS studies,[6, 30, 31] which proposed a $Cu^{1+}$ ground state. However, EPR data in solution showed the presence of $Cu^{1+}$ due to reduction of $Cu^{2+}$ to $Cu^{1+}$ in solution. It is likely that the XPS data suffered beam-induced photoreduction from the low-energy radiation. Interestingly, Cu L-edge data on CuS have a pre-edge feature that is similar in energy to the Cu $2p \rightarrow 3d^9$ feature in the discreet Cu-S systems (Figure S4 & S5) supporting the presence of $Cu^{2+}$ in CuS.

A comparison of the electronic structure developed here with the geometry reveals an interesting result. In CuS, the trigonal Cu centers are bound only to monosulfides, whereas the tetrahedral sites are bound to both mono- and disulfides. The presence of two pre-edge features in the S K-edge data indicates that, either both trigonal and tetrahedral sites have $Cu^{2+}$ centers, or only the tetrahedral site has $Cu^{2+}$ centers while the trigonal site has only $Cu^{1+}$ centers. Of these two models, the second is most consistent with all the spectroscopy presented here. Charge neutralization in CuS demands that one of the tetrahedral sites is $Cu^+$ and one is $Cu^{2+}$. Therefore the electronic structure can be described as $(Cu_{Td})^+(Cu_T)^+(Cu_{Td})^{2+}(S_2)^{2-}(S)^{2-}$ ($Cu_{Td}$ = tetrahedral, $Cu_T$ = trigonal). However, because the bond distances in all tetrahedral sites are equivalent, a charge delocalization between the two sites must be occurring, suggesting the more accurate description: $[(Cu_{Td})_2]^{3+}(Cu_T)^+(S_2)^{2-}(S)^{2-}$ (each $Cu_{Td}$ site is $Cu^{1.5+}$) It is also possible that the similarity in bond distances results from static disorder in the crystal structure leading to an average distance from crystallography. In either case, the crystal planes in CuS have alternating high and low charge on the Cu centers, which may contribute to internal energy transitions required for photoluminescence properties.

## 5. Conclusion

Previous x-ray spectroscopy data on copper sulfides are fraught with self-absorption issues and give mixed interpretations. Data have been typically interpreted qualitatively using fingerprinting techniques or by applying theoretical codes to simulate the spectra in order to obtain the electronic structure. In this study, an intermediate approach has been developed and applied to $Cu_2S$ and CuS. It is shown that comparative spectral peak assignment based on data from well-understood discreet molecules can be a powerful tool for electronic structure elucidation in unknown materials. This technique is shown to be successful in arriving at the electronic structure of the individual sites in the complex geometry of $Cu_2S$ and CuS and helped correlate their structure to function. In future studies, the electronic structures for $Cu_2S$ and CuS developed here will be extended to intermediate $Cu_{2-x}S$ systems to shed light on their unique physical properties.

This study demonstrates the strength of the molecular orbital theory approach to understanding bonding and electronic structure in repeating materials. Since electronic structures directly correlate to physical properties, the widespread use of this technique to material systems is proposed.

## Supplementary Material

Refer to Web version on PubMed Central for supplementary material.

## Acknowledgments

XAS data were measured at the Stanford Synchrotron Radiation Lightsource (SSRL), a Directorate of SLAC National Accelerator Laboratory and an Office of Science User Facility operated for the U.S. Department of Energy Office of Science by Stanford University. The SSRL Structural Molecular Biology Program is supported by the National Institutes of Health, National Center for Research Resources, Biomedical Technology Program and by the Department of Energy, Office of Biological and Environmental Research (BER). The publication was partially supported by Grant Number 5 P41 RR001209 from the National Center for Research Resources (NCRR), a component of the National Institutes of Health (NIH) and its contents are solely the responsibility of the authors and do not necessarily represent the official view of NCRR or NIH. PK and RN thank the DST, Government of India for financial support.

## Notes and References

1. Roseboom EH Jr. Econ. Geol. 1966; 61:641–672.
2. Zhao Y, Burda C. Energy Environ. Sci. 2012; 50:5564–5576.
3. Sagade AA, Sharma R, Sulaniya I. J. Appl. Phys. 2009; 105:043701.
4. Sakamoto T, Sunamura H, Kawaura H, Hasegawa T, Nakayama T, Aono M. Appl. Phys. Lett. 2003; 82:3032–3034.
5. Goble R. J. Can. Mineral. 1985; 23:61–76.
6. Wei Goh S, Buckley AN, Lamb RN. Miner. Eng. 2006; 19:204–208.
7. Nozaki H, Shibata K, Ohhashi N. J. Solid. State. Chem. 1991; 91:306–311.
8. Fjellvåg H, Grønvold F, Stølen S, Andresen AF, Müller-Käfer R, Simon S. Z. für Kristallogr. 1988; 184:111–121.
9. Gotsis HJ, Barnes AC, Strange P. J. Phys. Condens. Matt. 1992; 4:10461–10486.
10. Evans HT. Z. für Kristallogr. 1979; 150:299–320.
11. Lukashev P, LLambrecht WRL, Kotani T, van Schilfgaarde M. Phys. Rev. B: Condens. Matter. 2007; 76:195–202.
12. Okamata K, Kawai S. Jpn. J. Appl. Phys., Part 1. 1973; 12:1130–1138.
13. Itoh Y, Hayashi A, Yamagata H, Matsumura M, Koga K, Ueda Y. J. Phys. Soc. Jpn. 1996; 65:1953–1956.
14. Kumar P, Gusain M, Nagarajan R. Inorg. Chem. 2011; 50:3065–3070. [PubMed: 21370879]
15. Evans HT Jr. Science. 1979; 203:356–358. [PubMed: 17772445]
16. Kumar P, Nagarajan R. Inorg. Chem. 2011; 50:9204–9206. [PubMed: 21866946]
17. Cheng Z, Wang S, Wang Q, Geng B. Cryst. Eng. Commum. 2010; 12:144–159.
18. Ge ZH, Zhang BP, Chen YX, Yu ZX, Liu Y, Li JF. Chem. Commun. 2011; 47:12697–12699.
19. Wende H. Rep. Prog. Phys. 2004; 67:2105–2181.
20. Kau LS, Spira-Solomon DJ, Penner-Hahn JE, Hodgson KO, Solomon EI. J. Am. Chem. Soc. 1987; 109:6433–6442.
21. Stern, EA. EXAFS, SEXAFS and XANES. Koningsberger, DC.; Prins, R., editors. Vol. vol. 1. New York: John Wiley & Sons; 1988.
22. Tenderholt, A.; Hedman, B.; Hodgson, KO. X-ray Absorption Fine Structure - XAFS13. Stanford University; 2007.
23. Mustre de Leon J, Rehr JJ, Zabinsky SI, Albers RC. Phys. Rev. B: Condens. Matter. 1991; 44:4146–4156. [PubMed: 10000060]
24. Rehr JJ, Albers RC. Rev. Mod. Phys. 2000; 72:621–654.
25. George, GN. EXAFSPAK and EDG-FIT. Stanford, CA: Stanford Synchrotron Radiation Laboratory, Stanford Linear Accelerator Center; 2000.
26. Lee N, Petrenko T, Bergmann U, Neese F, DeBeer S. J. Am. Chem. Soc. 2010; 132:9715–9727. [PubMed: 20578760]
27. Sarangi R, York JT, Helton ME, Fujisawa K, Karlin KD, Tolman WB, Hodgson KO, Hedman B, Solomon EI. J. Am. Chem. Soc. 2008; 130:676–686. [PubMed: 18076173]

28. Sarangi R, Benfatto M, Hayakawa K, Bubacco L, Solomon EI, Hodgson KO, Hedman B. Inorg. Chem. 2005; 44:9652–9660. [PubMed: 16363833]
29. Donoghue PJ, Tehranchi J, Cramer CJ, Sarangi R, Solomon EI, Tolman WB. J. Am. Chem. Soc. 2011; 133:17602–17605. [PubMed: 22004091]
30. Luther GW 3rd, Theberge SM, Rozan TF, Rickard D, Rowlands CC, Oldroyd A. Environ. Sci. Technol. 2002; 36:394–402. [PubMed: 11871554]
31. Folmer JCC, Jellinek F. J. Less-Common Met. 1980; 76:153–162.
32. Shadle SE, Penner-Hahn JE, Schugar HJ, Hedman B, Hodgson KO, Solomon EI. J. Am. Chem. Soc. 1993; 115:767–776.
33. Kau LS, Hodgson KO, Solomon EI. J. Am. Chem. Soc. 1989; 111:7103–7109.
34. DuBois JL, Mukherjee P, Stack TDP, Hedman B, Solomon EI, Hodgson KO. J. Am. Chem. Soc. 2000; 122:5775–5787.
35. Szilagyi RK, Lim BS, Glaser T, Holm RH, Hedman B, Hodgson KO, Solomon EI. J. Am. Chem. Soc. 2003; 125:9158–9169. [PubMed: 15369373]
36. Solomon EI, Hedman B, Hodgson KO, Dey A, Szilagyi RK. Coord. Chem. Rev. 2005; 249:97–129.
37. Hedman B, Hodgson KO, Solomon EI. J. Am. Chem. Soc. 1990; 112:1643–1645.
38. Bergmann U, Glatzel P. Photosynth. Res. 2009; 102:255–266. [PubMed: 19705296]
39. Glatzel P, Bergmann U. Coord. Chem. Rev. 2005; 249:65–95.
40. Roemelt M, Beckwith MA, Duboc C, Collomb MN, Neese F, DeBeer S. Inorg. Chem. 2012; 51:680–687. [PubMed: 22145735]
41. Evans HT Jr. Nature. 1971; 232:69–70.

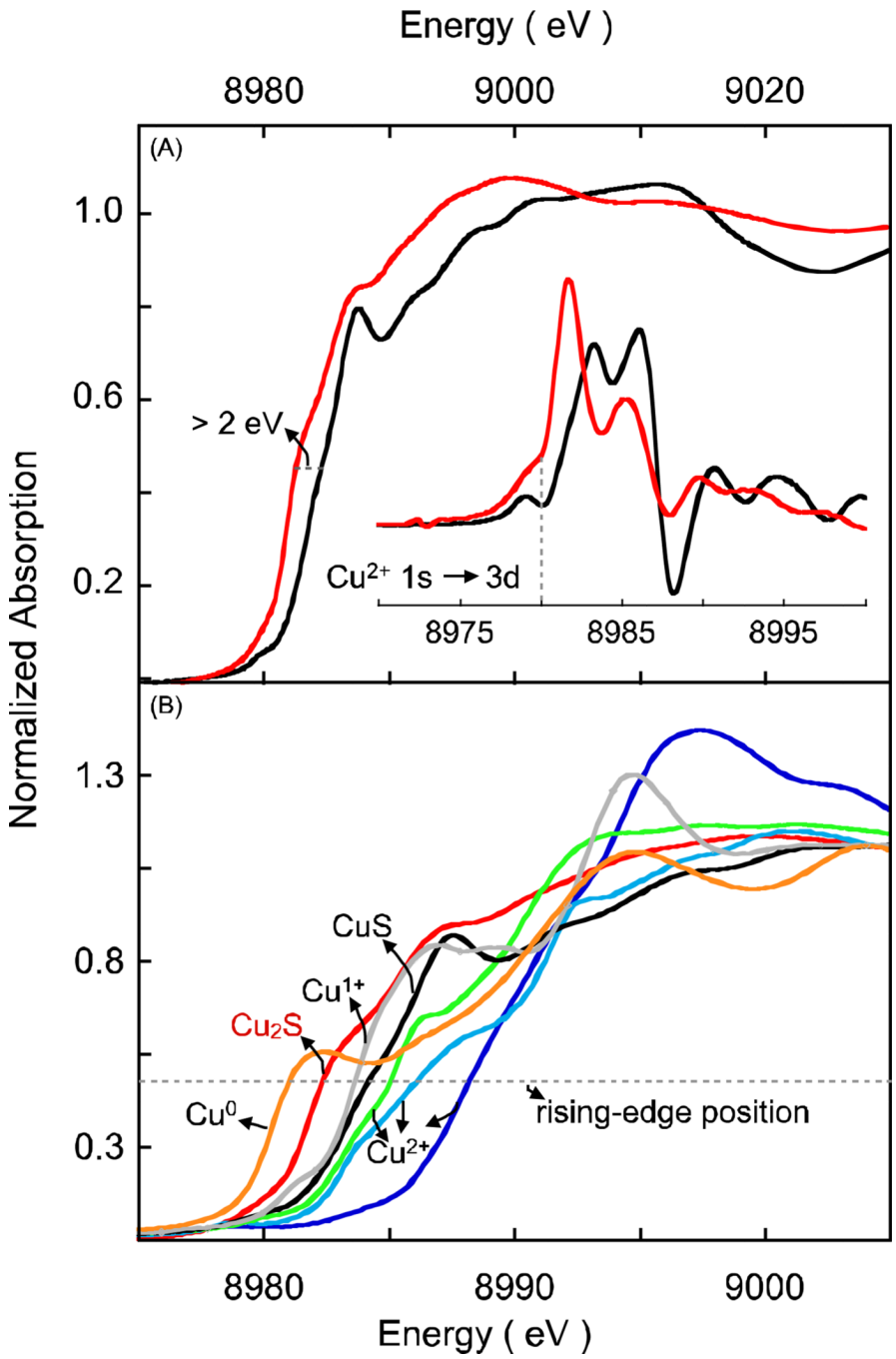


**Fig. 1.**

**(A)** The normalized Cu K-edge XAS spectra for $Cu_2S$ (—) and CuS (—). Horizontal dotted line shows the rising-edge energy shift. The inset shows the first derivative spectra. The vertical line shows the presence of a pre-edge feature corresponding to a Cu 1s → $3d^9$ transition. **(B)** Comparison of the Cu K-rising-edge region for Cu-S compounds: 1 (—)(no S ligand), 2 (—) (1 S ligand) 3, (—) (2 S ligands), CuS (—) (3.5 S ligands), 4 (—) (no S ligand), $Cu_2S$ (—) and copper foil (—). The horizontal dotted line represents the rising-edge intensity for energy measurement.

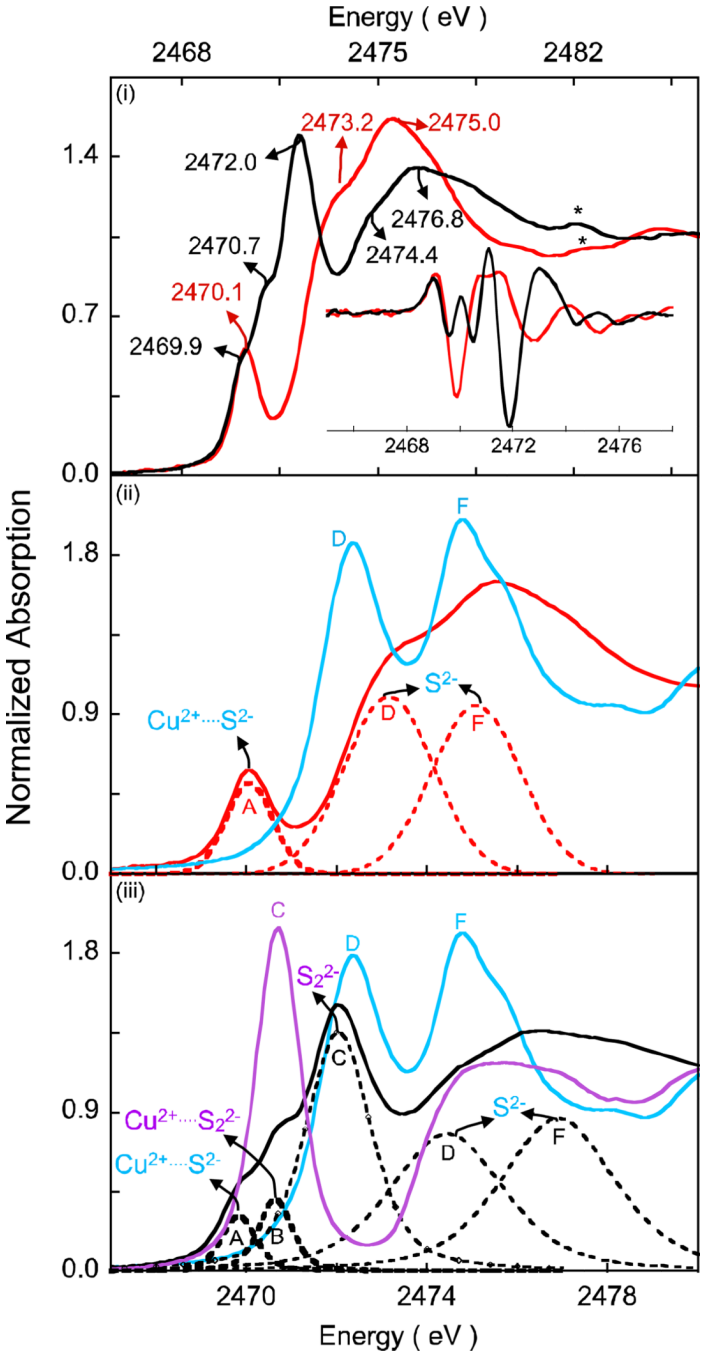


**Fig. 2.**

**(i)** The normalized S K-edge XAS spectra for $Cu_2S$ (—) and CuS (—). The inset shows the second derivative. **(ii)** $Cu_2S$ (—) and $Na_2S$ (—). **(iii)** CuS (—), $Na_2S$ (—) and $Na_2S_2$ (—). Both $Cu_2S$ and CuS data sets were fit using Pseudo-Voigt curves (dotted lines). Peaks related to those in $Na_2S$ and $Na_2S_2$ have been assigned the same alphabet. Peak A (in CuS and $Cu_2S$), which has no counterpart in $Na_2S$ results from a $S^{2-}$ 1s →$Cu^{2+}$ $3d^9$ transition. Peak B (in CuS) has no $Na_2S_2$ counterpart and results from a $S_2^{2-}$ 1s →$Cu^{2+}$ $3d^9$ transition.

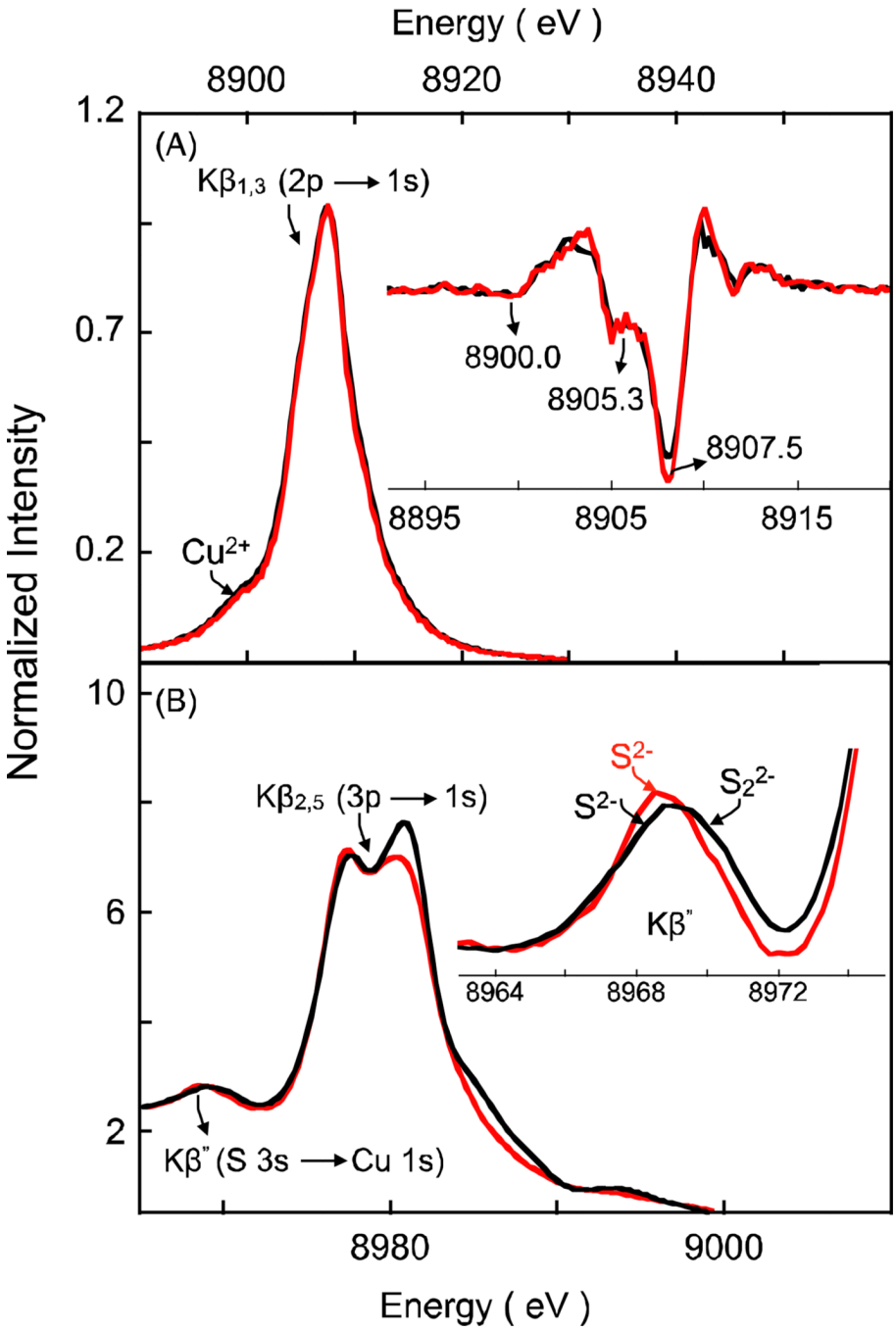


**Fig. 3.**

(A) The normalized Cu $K\beta_{1,3}$ data for $Cu_2S$ (—) and CuS (—). Inset shows the first derivative spectrum and the low-energy shoulder arising from a 3d hole (8900 eV). (B) The normalized Cu $K\beta_{2,5}$ region. Inset shows the valence to core Kβ" region. The broader CuS spectra indicate the presence of two distinct types of S species.

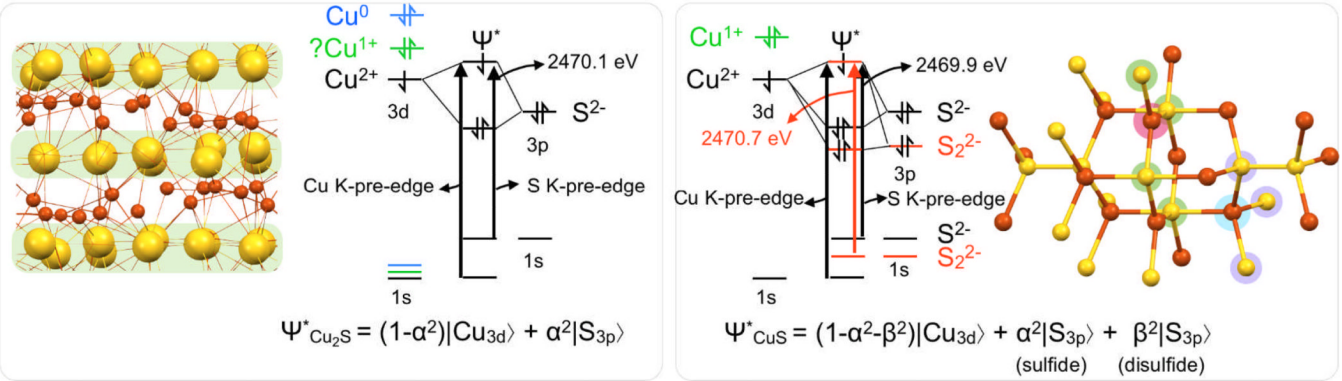


**Scheme 1.**

Crystal structures and MO diagram relevant for Cu K- and S K-edge X-ray absorption spectra for $Cu_2S$ and CuS. (left panel) The structure of $Cu_2S$ shows randomly packed Cu centers (orange) between sulfur planes (yellow) A close inspection of the crystal structure shows that Cu occurs in two kinds of triangular coordination one third of the metal atoms are in distorted triangular coordination within the hexagonal close-packed S layers, and the remaining are in triangular sites between the layers. (right panel) CuS has tetrahedral Cu centers (blue) bound to sulfide (green) and disulfide (violet) and trigonal centers (magenta) bound only to sulfides. For the MO diagrams, Cu oxidation states based on the XAS data are color-coded and their approximate relative d-band energies are shown. A partial ground state wave-function relevant to the XAS data is shown for both complexes. Since only the $Cu^{2+}$-$S^{2-}$/$Cu^{2+}$-$S_2^{2-}$ overlap leads to pre-edge features in the Cu and S K-edge, other $Cu^{1+}$/$Cu^{0}$-S interaction is omitted for clarity. For CuS the difference in energy of the 1s orbital of $S^{2-}$ and $S_2^{2-}$, leads to two S K-pre-edge features. A question mark near $Cu^{1+}$ represents lack of x-ray spectral evidence for quantitation.

**Table 1**

Cu and S K-edge energy positions

| | Cu K-edge Energy (eV)[a,b] | | | | | |
|---|---|---|---|---|---|---|
| | **$Cu_2S$** | **CuS** | **1** | **2** | **3** | **4** |
| Energy | 8982.2 | 8984.4 | 8988.2 | 8986.3 | 8985.1 | 8983.8 |

| | S K-edge Energy (eV)[a,b] | | | | |
|---|---|---|---|---|---|
| | **A** | **B** | **C** | **D** | **F** |
| $Cu_2S$ | 2470.1 | - | - | 2473.2 | 2475.0 |
| CuS | 2469.9 | 2470.7 | 2472.0 | 2474.4 | 2476.8 |
| $Na_2S_2$ | - | - | 2470.7 | - | - |
| $Na_2S$ | - | - | - | 2472.4 | 2474.8 |

[a] Energy precision >0.05 eV.

[b] Energy resolution ~0.1 eV. Data on **1, 2, 3, 4**, $Na_2S$ and $Na_2S_2$ have been reported previously.[27, 28, 32, 33, 35]